AIAA/AAS Astrodynamics Specialist Conference and Exhibit
5-8 August 2002, Monterey, California

AIAA 2002-4642

DESIGN OF A TETHER SLING FOR HUMAN TRANSPORTATION SYSTEMS BETWEEN EARTH AND MARS

Michael D. Jokic*
The University of Queensland, St Lucia, QLD 4072, Australia
and
James M. Longuski†
Purdue University, West Lafayette, IN 47907-1282, U.S.A.

In the current research, tether sling designs are developed for human transportation systems between Earth and Mars. Recent developments in the design of Cycler trajectories may benefit greatly from the construction of a tether sling facility on Phobos. The tether sling has the potential to launch vehicles from Mars with little, or no propellant required, since it is solar powered. For current trajectory designs and tether materials, it is shown that a tether sling facility is superior to chemical propulsion systems when multiple launches from Mars are considered.

INTRODUCTION

Puig-Suari et al.[1] propose a tether sling facility stationed at Phobos, and show that once built it could provide an inexhaustible means of transporting vehicles and astronauts. The sling is powered by solar cell arrays to initiate and maintain spin rate. For Hohmann transfers, the tether mass tends to be about the same as the propellant required in a chemical propulsion system. Kuchniki et al.[2] extend this work by examining the dynamics of a tether sling.

The mechanical advantages of tethers in space have been recognised for some time as reported in the overview by Penzo and Amman[3] and Cosmo and Lorenzini[4]. Tethers can be used for momentum transportation reducing, or eliminating, the need for precious, expendable propellant. Indeed, several concepts have been proposed that demonstrate the ability of tethered systems to act as transport facilities.[5-8]

The efficiency of tether transportation facilities is strongly dependant on their constituent material properties. Recently, great strides have been made in increasing material strength and lowering material density. Tether concept designs have employed a diverse range of materials that possess significantly better mechanical properties than metal cables.[1,9,10] The latest evolutions of tether materials, including Spectra and Zylon,[7] have extremely high strength-to-weight ratios. Current research into carbon nanotubes[11] suggests incredible strength potential for materials in the future.

Research into cyclical trajectories for transportation systems has been conducted since the 1960s, with some very interesting progress being made recently[14-21]. The aim of the research is to establish permanent, practical transportation systems that require little maintenance while achieving reasonable arrival and departure velocities for the vehicles involved.[22] By optimising these mission parameters, the propellant needed to conduct missions is reduced. With the potential benefits of cyclers in mind, McConaghy et al.[23] develop an analytical approach to identifying potential cycler trajectories.

In this paper, we investigate how advances in material science and trajectory design of cyclers may open the door to a highly efficient tether sling facility stationed on Phobos. The combination of cycler trajectories and a tether sling facility offers tremendous

* Ph.D. Candidate, Department of Mechanical Engineering. Member AIAA.
† Professor, School of Aeronautics and Astronautics, Associate Fellow AIAA, Member AAS.

potential in the design of a human transportation system between Earth and Mars.

MINIMUM-MASS SLING DESIGNS

Tapered Tether Analysis

In a tether sling facility the maximum tension occurs at the attachment point between the tether and the hub. Conversely, the minimum tension occurs at the end of the tether where the payload mass is attached (tip). Puig-Suari et al.[1] develop a tapered tether design that minimizes the mass of the tether by matching the cross-sectional area with the tension at a particular location along the tether. The following discussion outlines some of the key results from their analysis, which form the basis of the current tapered tether design.

For a location along the tether at a distance x from the hub, the tensile force is:

$$F_x = \int_x^l v^2 l^{-2} y \, dm_y + v^2 l^{-2} m_p \qquad (1)$$

where, l is the length of the tether, m_p is the mass of the payload. The term, dm_y, is the mass of a differential tether element located at a distance y along the tether. For a maximum allowable acceleration, and particular tip velocity, the length of the tether can determined using

$$l = v^2 / a_{max} \; . \qquad (2)$$

From Eq. (1), the cross-sectional area of the tether at location x can be represented as

$$A_x = F_x / \sigma = \left(v^2 / \sigma l\right)\left[\left(\rho / l\right) \int_x^l y A_y \, dy + m_p \right] \qquad (3)$$

where, A_y is the tether area at point y and σ is the tensile strength of the material. By differentiating Eq. (3) and then integrating, the expression for the tether area becomes

$$A_x = A_l \exp\left[\left(\rho v^2 / 2\sigma\right)\left(1 - x^2 l^{-2}\right)\right] \; . \qquad (4)$$

Here, A_l is the cross-sectional area of the tether at the end where the payload is attached. A_l is defined as:

$$A_l = m_p \left(v^2 / \sigma l\right). \qquad (5)$$

The mass of the tether can be represented as

$$m_t = \int_0^l \rho A_x \, dx \, . \qquad (6)$$

By substituting for A_x and performing an appropriate change of variables, the tether mass can be expressed in terms of the error function as

$$m_t = m_p v \left(\rho / 2\sigma\right)^{1/2} \pi^{1/2} \times \exp\left(\rho v^2 / 2\sigma\right) \mathrm{erf}\left(v \left(\rho / 2\sigma\right)^{1/2}\right), \qquad (7)$$

and in terms of a mass ratio as

$$m_t / m_p = \sqrt{\pi} \, v^* \exp\left(v^{*2}\right) \mathrm{erf}\left(v^*\right). \qquad (8)$$

The nondimensional velocity, v^*, is defined as

$$v^* = v \left(\rho / 2\sigma\right)^{1/2} = v / v_c \qquad (9)$$

where, v_c is the characteristic velocity of the tether material.

Puig-Suari et al. also derive an expression for the kinetic energy required for the tether sling. The moment of inertia of the system was found to be

$$I = m_p l^2 \left(\pi^{1/2} / 2v^*\right) \exp\left(v^{*2}\right) \mathrm{erf}\left(v^*\right) \qquad (10)$$

which leads to the expression for the rotational kinetic energy required for a desired tip velocity,

$$E_{req} = \left(\pi^{1/2} / 4\right) \exp\left(v^{*2}\right) \mathrm{erf}\left(v^*\right) v^* v_c^2 \qquad (11)$$

The amount of power supplied by solar panels to generate the required rotational kinetic energy is

$$E_{solar} = \left(P / A\right) A t = P t \qquad (12)$$

where, A is the area of the solar array, t is time and P/A represents the output of the solar array per unit area.

Mission Scenarios

In sizing the tether sling facility, two scenarios are considered. The first employs the tether sling as a launch facility for directly transferring material between Mars and Earth. This scenario can be achieved through a semi-cycler trajectory, a Hohmann transfer, a rapid transfer trajectory (with a time-of-flight less than half a year), or Mars free-return trajectories. In each case, the vehicle being launched is assumed to have a mass of 70 metric tons. For comparison, the mass needed to achieve the same launch conditions for a chemical rocket employing liquid oxygen and methane (LOX/CH_4) is included. The ratio of the structural mass to the propellant mass is assumed to 0.15 for the single stage rocket.

The second scenario considers the use of the tether sling to launch taxi vehicles, which rendezvous with a cycler vehicle as it performs a flyby of Mars. In this scenario, the taxi mass is about 11 metric tons. Two rocket models, which use LOX/CH_4 propellant, are

included for comparison. The first model considers a single stage rocket, while the second is staged to closely match the Mars taxi system proposed by Knock.[19] Figure 1 shows the propellant mass performance profile of the Mars taxi model used in the current investigation.

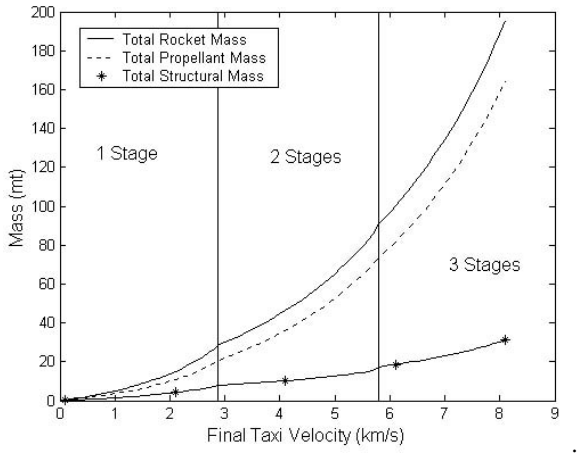

Figure 1: Mass profile of the taxi rocket model.

Tether Sling Performance

The performance of the tether sling, in terms of mass, is dependent on the mechanical properties of the tether material. Table 1 lists the mechanical properties for several tether materials that have been implemented in the literature.

Table 1: Tether material mechanical properties

Material	Spectra 2000	Zylon	Kevlar	Hercules IM7
Tensile Strength (GPa)	3.51	5.8	2.8	4.82
Density (kg/m^3)	970	1560	1450	1550

Figure 2 presents the mass performance of the tether sling relative to the propellant required by a single stage rocket to produce the same final velocity. Clearly, the materials with high strength-to-weight ratios produce a more favourable mass ratio. This is particularly evident at higher launch velocities. The 2010 material is based upon a linear projection of the strength-to-weight ratios of materials that have become available. Notably, the strength-to-weight ratios of the Spectra 2000 and Zylon materials are similar, resulting in closely matching mass-performance profiles. Similar trends are observable in Fig. 3, which represents the mass-performance of the tether sling relative to the propellant requirements calculated using the Mars taxi model. In this instance, however, the lower propellant needs of the multi-stage rocket results in tether mass to propellant mass ratios than for the single stage rocket model at high launch velocities (>5 km/s).

Examining Eq. 7 reveals that the tether mass is proportional to the payload mass. The effect of slinging an astrotel as opposed to the taxi vehicle is evident in Fig. 4. The curves in Fig. 4, which correspond to the 5 different materials, increase to a mass ratio of 20 at lower sling velocities than in the Figs. 2 and 3. This implies that there is a lower limit for the range of feasible operating sling velocities for an astrotel payload than for a taxi payload.

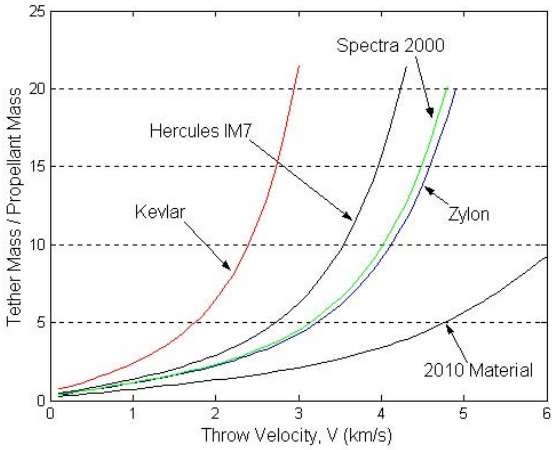

.Figure 2: Tether sling mass performance, for the taxi vehicle, relative to propellant mass using a single stage rocket.

Table 2 presents designs of a tether sling facility stationed on Phobos for specific mission scenarios. Several transfer trajectories are represented in the table. Both direct mass transfers between Mars and Earth, and rendezvous with astrotels on cycler trajectories are investigated. In all cases, the worst case to maintain the particular trajectory for the proposed launch dates and synodic periods are considered. In all cases, the mechanical properties of Zylon have been implemented.

Each of the trajectories classified in the "direct transfer category" require an astrotel to be launched using the tether sling. First among these are the trajectories classified as semi-cycler 1 and semi-cycler 2. The semi-cycler trajectories involve a launch and arrival at Mars with flybys of Earth. Next, are two Mars-to-Earth transfers corresponding to a Hohmann

transfer and a transfer with a time of flight between Mars and Earth of less than half a year. Finally, an Earth free-return trajectory is considered for a launch from Mars using a tether sling.

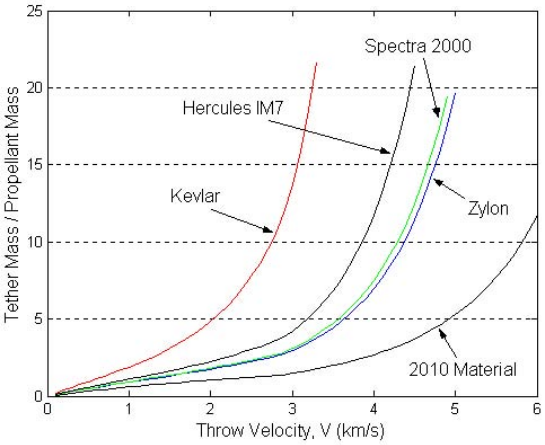

Figure 3: Tether sling mass performance, for the taxi vehicle, relative to propellant mass using the taxi model.

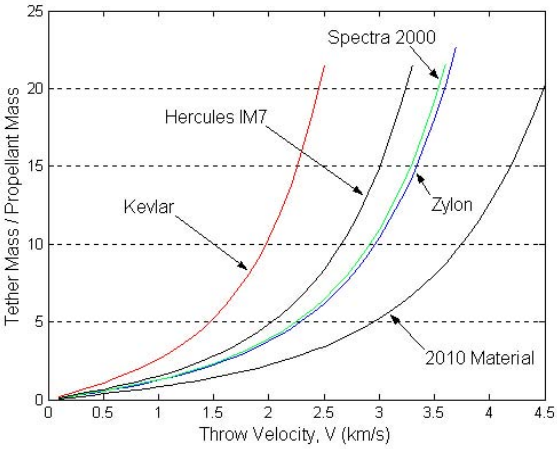

Figure 4: Tether sling mass performance, for the astrotel, relative to propellant mass using a single stage rocket.

As can be seen from Table 2, the tether sling compares favourably to the rocket in terms of mass for the direct transfer trajectories. For these trajectories, the largest tether-mass-to-propellant-mass ratio is 3.5. Reflecting on the fact that the tether sling is a reusable system, the tether will produce significant mass savings after the fourth launch. The propellant mass requirements to achieve the desired velocities are calculated using a single stage rocket model. As stated in Eq. 2, the tether length is a function of the sling velocity and the maximum allowable acceleration of the payload. The tether lengths for the direct transfer scenarios range from 70 to 181 km. In all cases, it is assumed that the tether sling facility must impart enough change in velocity to provide the payload with the appropriate hyperbolic excess speed after launching from Phobos.

The final three trajectories presented in Table 2 represent scenarios where the tether sling launches a taxi vehicle to rendezvous with an astrotel in a cycler orbit. Each of the hyperbolic excess speeds listed have been obtained from research into optimising the Aldrin Cycler[24] and developing alternative cycler trajectories.[22, 23] The Aldrin Cycler system consists of two astrotels called an up-cycler and a down-cycler. The up-cycler is in an elliptic orbit about the sun such that it has a type 1 transfer (<180°) from Earth to Mars every synodic period (2.14 years). Conversely, the down-cycler has a type 1 transfer from Mars to Earth every synodic period. Patching semi-cycler trajectories together has been an approach adopted[22] to develop cycler trajectories. It is from this area of research that the remaining cycler trajectories in Table 2 have originated. Repeating cycles of Mars-Earth-Earth-Mars (M-E-E-M) and Earth-Mars-Mars-Earth (E-M-M-E) are two potential candidates for cycler trajectories.

As the physical characteristics of the tether sling are highly dependent on the required velocity at the tether tip, the size of the tether needed for the Aldrin Cycler is prohibitively large. For the other cycler trajectories, however, the tether sling performance is extremely encouraging. The mass ratios for the patched semi-cycler trajectories are both less than 10, which is reasonable, allowing for the reusability of the tether system.

Table 2: Tether sling system properties for transfer trajectories between Earth and Mars

System Parameters	Units	Semi-cycler 1	Semi-cycler 2	M-E Hohmann	M-E (<1/2 year)	M-E-M	3 Synodic Period E-M-M-E	M-E-E-M Semi-Cycler	Aldrin Cycler
Payload Mass	mt	70	70	70	70	70	11.177	11.177	11.177
V_∞	km/s	2.76	3.96	1.88	3	4	5.56	4.8	11.94
ΔV	km/s	1.96	2.84	1.42	2.12	2.88	4.19	3.54	10.18
Max. Accel.	g	3	3	3	3	3	3	3	3
I_{sp}	s	379	379	379	379	379	379	379	379
Single Stage Prop.	mt	54	97	35	61	99	34	23	invalid
Taxi Model Prop.	mt	-	-	-	-	-	41	31	483
l	km	130.0	275.0	68.8	153.0	281.2	597.4	424.8	3519.5
Diameter at End	cm	2.1	2.1	2.1	2.1	2.1	0.8	0.8	0.8
Diameter at Hub	cm	2.7	3.7	2.4	2.9	3.7	2.8	2.0	897.3
Tether Mass	mt	103	330	46	129	344	314	129	8.2E07
μ_{single} [a]		1.90	3.40	1.31	2.12	3.47	9.23	5.52	invalid
μ_{taxi} [b]		-	-	-	-	-	7.59	4.18	1.71E05

[a] μ_{single} = tether mass to single-stage propellant mass ratio.

[b] μ_{taxi} = tether mass to taxi model propellant mass ratio.

PRACTICAL SLING DESIGNS

The minimum-mass design does not allow for errors in the manufacture of the tether, which may result in fluctuations in the cross-sectional area along the length of the tether. Nor does the minimum-mass design consider the effect of including a safety factor. The following analysis considers the implications of the inclusion of the first of these design elements on the mass of the tether sling.

Tapered Tether Analysis

The cross-sectional area of the tapered tether can take several profiles depending upon whether a cable or tape tether is adopted. Figure 5 depicts potential cross sections for each of these tether types. In order to keep the analysis of the effect of manufacturing errors general, fluctuations in cross-sectional area have been considered as opposed to dimensional tolerances.

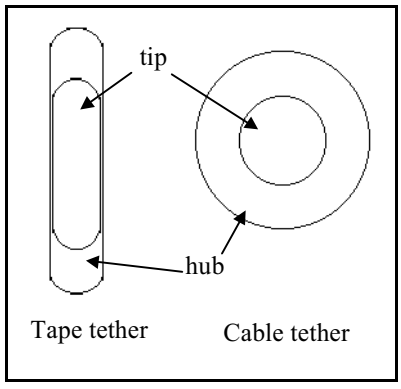

Figure 5: Possible tapered tether cross-sections at the tip and hub attachment point.

To take into account errors in the cross-sectional area, the minimum producible area at a given location must be capable of withstanding the tensile forces generated by the maximum tether area at all other locations. By this principle, the area at the end of tether calculated by the minimum-mass analysis becomes the minimum allowable area at that location. The minimum tip area relates to the nominal design area by

$$A_{t\,min} = m_p\left(v^2/\sigma 1\right) = \left(1-\Delta\right) A_{t\,nom}\,. \quad (13)$$

This is assuming that any cross section can fluctuate by $\pm\Delta\times 100\%$. Subsequently, the maximum producible area at the tether tip is

$$A_{t\,max} = \left(1+\Delta\right)\left(1-\Delta\right)^{-1} A_{t\,min}\,. \quad (14)$$

Considering the extreme case where the maximum area is produced at all locations along the tether allows the development of an appropriate design. This is the situation which will produce the most tensile force, and largest tether mass. Figure 6 shows the worst-case scenario where the maximum tether profile must be supported by a minimum tether profile in a cable-tether sling.

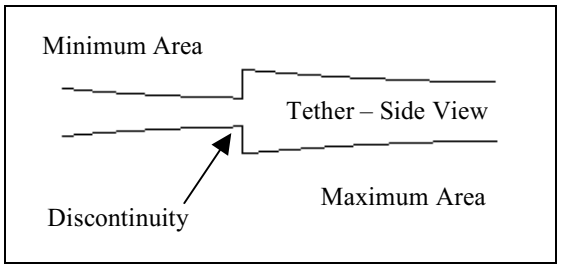

Figure 6: A worst-case discontinuity in the cross-sectional area of a tether sling.

Following the minimum-mass analysis, the maximum cross-sectional area at any location along the tether is

$$A_{x\,max} = A_t \exp\left[\left(1+\Delta\right)\left(1-\Delta\right)^{-1}\left(v^2\rho/2\sigma\right)\left(1-x^2 l^{-2}\right)\right]. \quad (15)$$

The corresponding maximum tether mass is defined as

$$m_{t\,max} = A_t \exp\left[\left(1+\Delta/1-\Delta\right)\left(v^2\rho/2\sigma\right)\right]\times \int_0^l \exp\left[-\left(1+\Delta/1-\Delta\right)\left(v^2\rho/2\sigma\right)x^2 l^{-2}\right]. \quad (16)$$

Again using an appropriate change of variables, the mass ratio can be determined from

$$m_{t\,max}/m_p = \pi^{1/2} v^* \left(1-\Delta/1+\Delta\right)^{1/2} \exp\left[v^{*2}\left(1+\Delta/1-\Delta\right)\right]\ \mathrm{erf}\left[v^*\left(1+\Delta/1-\Delta\right)^{1/2}\right]. \quad (17)$$

The implications of the potential fluctuations in cross-sectional area to the mass of the tether become evident by examining Fig. 7. The figure represents nondimensionally, the radius of the tether at each location along a cable tether sling for both the practical and minimum-mass designs. As expected, the radius for the design, including fluctuations in area, is greater at nearly all locations than the minimum-mass design. The only overlap between the designs occurs at the tether tip where the minimum manufactured radius is equal to the minimum mass value. The difference between the tether radius produced from the minium-mass and practical design techniques is dependent on the area fluctuation factor, Δ. For the results depicted in Fig. 7, a value of 0.05 is used for the fluctuation factor.

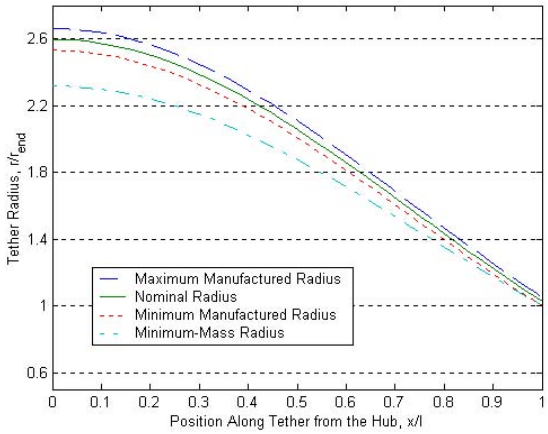

Figure 7: Non-dimensional tether radius versus non-dimensional position along the tether.

Table 3: Tether sling system properties for transfer trajectories between Earth and Mars allowing for fluctuations in the cross-sectional area of the tether.

System Parameters	Units	Semi-cycler 1	Semi-cycler 2	M-E Hohmann	M-E (<1/2 year)	M-E-M	3 Synodic Period E-M-M-E	M-E-E-M Semi-Cycler	Aldrin Cycler
Payload Mass	mt	70	70	70	70	70	11.177	11.177	11.177
V_∞	km/s	2.76	3.96	1.88	3	4	5.56	4.8	11.94
ΔV	km/s	1.96	2.84	1.42	2.12	2.88	4.19	3.54	10.18
l	km	130.0	275.0	68.8	153.0	281.2	597.4	424.8	3519.5
Δ		0.05	0.05	0.05	0.05	0.05	0.05	0.05	0.05
Max. Diam. at End	cm	2.24	2.24	2.24	2.24	2.24	0.89	0.89	0.89
Nom. Diam. at End	cm	2.13	2.13	2.13	2.13	2.13	0.85	0.85	0.85
Min. Diam. at End	cm	2.02	2.02	2.02	2.02	2.02	0.81	0.81	0.81
Max. Diam. at Hub	cm	2.97	4.08	2.60	3.12	4.13	3.30	2.26	1963.16
Nom. Diam. at Hub	cm	2.83	3.88	2.47	2.97	3.94	3.14	2.15	1869.68
Min. Diam. at Hub	cm	2.69	3.69	2.35	2.83	3.74	2.98	2.05	1776.19
Max. Tether Mass	mt	107	360	47	135	376	386	148	3.4.E08
Max. μ_{single} [a]		1.97	3.70	1.33	2.21	3.79	11.35	6.35	Invalid
Max. μ_{taxi} [b]		-	-	-	-	-	9.33	4.81	7.03E05

[a] μ_{single} = tether mass to single-stage propellant mass ratio.

[b] μ_{taxi} = tether mass to taxi model propellant mass ratio.

The inclusion of fluctuations in the cross-sectional area of the tether sling alters the results obtained for the transfer trajectories between Earth and Mars. Table 3 contains updated results from those presented in Table 2 for the minimum-mass analysis. The details of the trajectories and the corresponding propellant requirements are unchanged. However, the physical dimensions and mass of the tether have increased. For each of the trajectories listed, three diameters are included for the tether tip and hub attachment point. These values correspond to the maximum, minimum and nominal manufactured diameters of the tether. For the purposes of discussing the worst tether-sling-mass performance, the maximum tether mass and mass ratio results are included. For the lower throw velocity scenarios, the effect of the adjusted tether design on the tether mass to propellant mass ratio is quite small. In most cases, the mass ratio continues to remain under 10. The exceptions to this are the Aldrin Cycler and the M-E-E-M patched semi-cycler trajectories. In the case of the patched semi-cycler, the mass ratio has increased, with respect to the single stage rocket model, from 9.23 to 11.35.

Incorporating a safety factor into the design results in an increase in the mass of the tether and, subsequently, an increase in the mass ratio. For the development of an effective tether sling, or any mass-sensitive tether application, non-ideal designs must be considered. The limitations of the manufacturing processes and accounting for uncertainties through the inlcusion of an appropriate safety factor are crucial issues in practice.

CONCLUSIONS

The current research investigates the use of a tether sling facility in human transportation systems between Earth and Mars. For the mission scenarios and trajectories presented, the tether sling mass is up to 10 times the equivalent propellant mass requirements. This is significant due to the fact that the sling is capable of multiple launches, which will eventually result in enormous mass savings. With continued advancements in the field of material science and improvements in trajectory designs, the mass performance of a tether sling facility will greatly improve. Ultimately, a tether sling facility on Phobos may be of tremendous benefit to advancing the human exploration of space.

ACKNOWLEDGEMENTS

This work was made possible, in part, through the Graduate School Research Travel Award (GSRTA) scheme of the University of Queensland Graduate School.

REFERENCES

[1]Puig-Suari, J., Longuski, J. M. and Tragesser, S. G., "A Tether Sling for Lunar and Interplanetary Exploration", *Acta Astronautica*, Vol. 36, 1995, pp. 291-295.

[2]Kuchnicki, S. N., Tragesser, S. G. and Longuski, J. M., "Dynamics of a Tether Sling", in *AAS/AIAA Astrodynamics Specialist Conference*, Paper AAS 97-605, Sun Valley, ID, 1997.

[3]Penzo, P. A. and Amman, P. W. (Editors), *Tethers in Space Handbook, 2nd ed.*, Office of Space Flight Advanced Programmes, NASA, Washington, DC, 1989.

[4]Cosmo, M. L. and Lorenzini, E. C. (Editors), *Tethers in Space Handbook, 3rd ed.*, Smithsonian Astrophysical Observatory, 1997.

[5]Hoyt, R. P. and Uphoff, C. W., "Cislunar Tether Transport System", *Journal of Spacecraft and Rockets*, Vol. 37, no. 2, 2000, pp. 177-186.

[6]Forward, R. and Nordley, G., "Mars-Earth Rapid Interplanetary Tether Transport (MERITT) System: Initial Feasibility Study", 35th *AIAA/ASME/SAE/ASEE Joint Propulsion Conference and Exhibit*, AIAA Paper 99-2839, Los Angeles, CA, 1999.

[7]Bogar, T. J., Bangham, M. E., Forward, R. L., Lewis, M.J., "Hypersonic Airplane Space Tether Orbital Launch (HASTOL) System: Interim Study Results", *9th International Space Planes and Hypersonic Systems and Technologies Conference*, AIAA-99-4802, AIAA, Norfolk, VA, 1999.

[8]Colombo, G., "The use of Tether for Payload Orbit Transfer", NASA, Report N82-26705, 1982.

[9]Pasca, M. and Lorenzini, E., "Collection of Martian Atmospheric Dust with a Low Altitude Tethered Probe", *Advances in the Astronautical Sciences*, Vol. 75, 1991, pp. 1121-1139.

[10]Pasca, M. and Lorenzini Enrico, C., "Optimization of a Low Altitude Tethered Probe for Martian Atmospheric Dust Collection", *Journal of the Astronautical Sciences*, Vol. 44, 1996, pp. 191-205.

[11]Smitherman, D. V. J., "Space Elevators: An Advanced Earth-Space Infrastructure for the New Millennium", Report NASA/CP-2000-210429, NASA Marshall Space Flight Center, 2000.

[12]Hollister, W. M., "Castles in Space," *Astronautica Acta*, Vol. 14, pp. 311-316, 1969.

[13]Rall, C. S. and Hollister, W. M., "Free-Fall Periodic Orbits Connecting Earth and Mars," *AIAA 9th Aerospace Sciences Meeting*, AIAA Paper No 71-92, New York, NY, Jan. 25-27, 1971.

[14]Friedlander, A. L., Niehoff, J. C., Byrnes, D. V., and Longuski, J. M., "Circulating Transportation Orbits Between Earth and Mars," *AIAA/AAS Astrodynamics Conference*, AIAA Paper 86-2009, Williamsburg, VA, Aug. 18-20, 1986.

[15]Aldrin, B., "Cyclic Trajectory Concepts," *SAIC presentation to the Interplanetary Rapid Transit Study Meeting*, Jet Propulsion Laboratory, Pasadena, CA, Oct. 28, 1985.

[16]Byrnes, D. V., Longuski, J. M., and Aldrin, B., "Cycler Orbit Between Earth and Mars," Journal of Spacecraft and Rockets, Vol. 30, No. 3, 1993, pp. 334-336.

[17]Hoffman, S. J., Friedlander, A. L., and Nock, K. T., "Transportation Node Performance Comparison for a Sustained Manned Mars Base," *AIAA/AAS Astrodynamics Conference*, Williamsburg, AIAA Paper 86-2016, VA, Aug. 18-20, 1986.

[18]Bishop, R. H., Byrnes, D. V., Newman, D. J., Carr, C. E., and Aldrin, B., "Earth-Mars Transportation Opportunities: Promising Options for Interplanetary Transportation," The Richard H. Battin Astrodynamics Conference, AAS Paper 00-255, College Station, TX, Mar. 20-21, 2000.

[19]Nock, K. T., "Cyclical Visits to Mars via Astronaut Hotels," Phase I Final Report, NASA Institute for Advanced Concepts, Universities Space Research Association Research Grant 07600-049, Global Aerospace Corporation, Altadena, CA, Nov. 30, 2000.

[20]Nock, K. T., and Friedlander, A. L., "Elements of a Mars Transportation System," *Acta Astronautica*, Vol. 15, No. 6/7, 1987, pp. 505-522.

[21]Aldrin, B., Byrnes, D., Jones, R., and Davis, H., "Evolutionary Space Transportation Plan for Mars Cycling Concepts," AIAA Paper 2001-4677, Albuquerque, NM, 2001.

[22]Chen, J. K., Landau, D. F., McConaghy, T. T., Masataka, O. and Longuski, J. M., "Trajectory Analysis and Design of Mars Cyclers: Preliminary Assessment", Purdue University, West Lafayette, IN, 2001.

[23]McConaghy, T. T., Longuski, J. M. and Byrnes, D. V., "Analysis of a Broad Class of Earth-Mars Cycler Trajectories", *AIAA/AAS Astrodynamics Specialist Conference*, AIAA Paper 2002-4420, Monterey, CA, Aug. 5-8, 2002.

[24]Chen, K. J., Okutsu, M., McConaghy, T. T. and Longuski, J. M., "Cyclical Visits to Mars via Astronaut Hotels", Purdue University, West Lafayette, IN, 2001.